Title

Quantification of Nonenhancing Tumor Burden in Gliomas Using Effective T2 Maps Derived from Dual-Echo Turbo Spin-Echo MRI

Journal

Clinical Cancer Research, 21(19)

ISSN

1078-0432

Authors

Ellingson, Benjamin M
Lai, Albert
Nguyen, Huytram N
et al.

Publication Date

2015-10-01

DOI

10.1158/1078-0432.ccr-14-2862

Peer reviewed

Published OnlineFirst April 21, 2015; DOI: 10.1158/1078-0432.CCR-14-2862

Personalized Medicine and Imaging

Clinical Cancer Research

Quantification of Nonenhancing Tumor Burden in Gliomas Using Effective T_2 Maps Derived from Dual-Echo Turbo Spin-Echo MRI

Benjamin M. Ellingson[1,2,3,4,5,6], Albert Lai[1,6,7], Huytram N. Nguyen[1,7], Phioanh L. Nghiemphu[1,6,7], Whitney B. Pope[2], and Timothy F. Cloughesy[1,6,7]

Abstract

Purpose: Evaluation of nonenhancing tumor (NET) burden is an important yet challenging part of brain tumor response assessment. This study focuses on using dual-echo turbo spin-echo MRI as a means of quickly estimating tissue T_2, which can be used to objectively define NET burden.

Experimental Design: A series of experiments were performed to establish the use of T_2 maps for defining NET burden. First, variation in T_2 was determined using the American College of Radiology (ACR) water phantoms in 16 scanners evaluated over 3 years. Next, the sensitivity and specificity of T_2 maps for delineating NET from other tissues were examined. Then, T_2-defined NET was used to predict survival in separate subsets of patients with glioblastoma treated with radiotherapy, concurrent radiation, and chemotherapy, or bevacizumab at recurrence.

Results: Variability in T_2 in the ACR phantom was 3% to 5%. In training data, ROC analysis suggested that 125 ms < T_2 < 250 ms could delineate NET with a sensitivity of >90% and specificity of >65%. Using this criterion, NET burden after completion of radiotherapy alone, or concurrent radiotherapy, and chemotherapy was shown to be predictive of survival (Cox, $P < 0.05$), and the change in NET volume before and after bevacizumab therapy in recurrent glioblastoma was also a predictive of survival ($P < 0.05$).

Conclusions: T_2 maps using dual-echo data are feasible, stable, and can be used to objectively define NET burden for use in brain tumor characterization, prognosis, and response assessment. The use of effective T_2 maps for defining NET burden should be validated in a randomized, clinical trial. *Clin Cancer Res; 21(19); 4373–83. ©2015 AACR.*

Introduction

The use of contrast-enhancing tumor burden has been the standard for brain tumor response assessment for more than 60 years; however, approximately 30% to 40% of patients are estimated to experience nonenhancing tumor (NET) progression prior to changes in contrast enhancement (1, 2). Although contrast enhancing tumor is thought to represent the most aggressive portion of the tumor (3, 4) and a large percentage of high-grade gliomas have a significant enhancing component (5), malignant gliomas are known to contain proportions of both neovascularized and infiltrative tumor (6, 7). Because a substantial proportion of treated tumors can have NET progression (1, 6), and progression of NET can lead to neurologic decline, there is an emergent need for consideration of NET burden in an updated response criteria in neuro-oncology, which was further outlined in the Jumpstarting Brain Tumor Drug Development Coalition and Food and Drug Administration (FDA) Workshop in January 2014 (8, 9).

Damadian (10) first documented distinct differences in proton relaxation rates between normal and cancerous tissues as early as 1971, which was also confirmed by various groups in the subsequent years (11–15). Clinical diagnosis and monitoring of brain tumors with MRI, however, remains reliant on the use of T_1 or T_2 "weighted" images, which express qualitative changes in the MR signal. T_2 relaxometry can theoretically be performed using a simple modification to the standard T_2-weighted MRI sequence that results in obtaining multiple images at various echo times (TE), which is essentially "free" information (i.e., no substantial added scan time). This information can in theory be used to create quantitative maps of T_2, which is specific for various tissue types, including cancer, but relatively independent of MR acquisition parameters, such as TE. For example, an early study by Hoehn-Berlage and colleagues (16) correlated tumor tissue in a cat model with quantitative T_2 maps at 4.7T and demonstrated that $T_{2edema} > T_{2tumor} > T_{2normal\ WM}$, consistent with the current clinical

[1]UCLA Neuro-Oncology Program, David Geffen School of Medicine, University of California, Los Angeles, California. [2]Department of Radiological Sciences, David Geffen School of Medicine, University of California, Los Angeles, California. [3]Biomedical Physics Program, David Geffen School of Medicine, University of California, Los Angeles, California. [4]Department of Bioengineering, Henry Samueli School of Engineering and Applied Science, University of California, Los Angeles, California. [5]UCLA Brain Research Institute, David Geffen School of Medicine, University of California, Los Angeles, California. [6]Jonsson Comprehensive Cancer Center, University of California, Los Angeles, California. [7]Department of Neurology, David Geffen School of Medicine, University of California, Los Angeles, California.

Note: Supplementary data for this article are available at Clinical Cancer Research Online (http://clincancerres.aacrjournals.org/).

Corresponding Author: Benjamin M. Ellingson, David Geffen School of Medicine, University of California, Los Angeles, 924 Westwood Boulevard, Suite 615, Los Angeles, CA 90024. Phone: 310-481-7572; Fax: 310-794-2796; E-mail: bellingson@mednet.ucla.edu

doi: 10.1158/1078-0432.CCR-14-2862

Published OnlineFirst April 21, 2015; DOI: 10.1158/1078-0432.CCR-14-2862

Translational Relevance

This study provides a comprehensive evaluation of the use of T_2 relaxation rates estimated from dual-echo turbo spin-echo images to objectively define nonenhancing tumor (NET) burden in patients with gliomas. Results suggest T_2 measurements are relatively stable across scanners and may be useful for delineating NET from other tissues. Results also suggest that the use of T_2-defined NET burden may be useful for prognostic and response assessment purposes.

observation of moderately hyperintense lesions on T_2-weighted images being associated with NET (17). This difference in T_2 relaxation rates between edema, tumor, and normal tissues has been characterized in both rodent models (18) and human tumors (19–21). In addition, studies have shown that T_2 relaxation tends to be monoexponential (16), suggesting evaluation of NET may be possible with a single T_2 parameter. We hypothesize that "effective" T_2 relaxometry performed using the turbo spin-echo (TSE) may be useful for objectively defining NET tissue using a specific range of T_2 values.

Accurate measurements of T_2 relaxation times typically involve using relatively time inefficient multiecho Carr–Purcell–Meiboom–Gill (CPMG) sequences. Dual-echo TSE sequences are an attractive clinical alternative to CPMG sequences (22, 23), allowing for "effective" T_2 estimation (T_2^{eff}) in clinically feasible scan times and clinically useful spatial coverage for a variety of anatomical locations (24–28). In this study, we examined the stability of T_2^{eff} estimates in a standard water phantom across a variety of scanners, used dual-echo TSE data from 50 patients with a range of glioma grades scanned on a variety of scanners and field strengths to define T_2^{eff} characteristics for various tissues, then applied this information to a cohort of newly diagnosed glioblastoma patients treated with radiotherapy, a cohort of newly diagnosed glioblastoma patients treated with concurrent radiotherapy and temozolomide, and a set of recurrent glioblastoma patients treated with bevacizumab to determine whether the volume of T_2^{eff}-defined NET can be used to predict progression-free survival (PFS) and overall survival (OS).

Materials and Methods

Summary of experiments

A series of experiments were performed in this study to establish the use of T_2^{eff} in defining NET burden for use in quantification of tumor burden and response assessment. First, the normal variation expected in T_2^{eff} estimates was determined on the American College of Radiology (ACR) standard water phantom using dual-echo TSE images collected for 16 different scanners and field strengths. Next, the sensitivity and specificity of T_2^{eff} in delineating NET from edema, necrotic tissue, and normal-appearing brain tissue were estimated in a training set of 50 glioma patients in order to define cutoffs for defining NET. Using thresholds defined by these training data, we examined an independent set of 25 newly diagnosed glioblastoma patients who were treated with radiotherapy, but no concurrent temozolomide and never were exposed to bevacizumab, to determine whether NET burden evaluated at this post-radiotherapy time point could predict PFS and OS. Then, another independent set of 35 glioblastoma patients treated with concurrent radiotherapy and temozolomide, but were never exposed to bevacizumab, were evaluated at the post-radiotherapy time point to determine whether NET burden prior to adjuvant therapy could predict PFS and OS. Finally, we examined a set of 24 recurrent glioblastoma patients treated with bevacizumab to determine whether the change in NET burden could be used to predict PFS and OS.

Phantom studies

A total of 16 MRI scanners spanning various field strengths and manufacturers were evaluated from 2010 to 2015 using the ACR accreditation phantom (Fig. 1). Dual-echo TSE data were acquired according to ACR guidelines (www.acr.org/~/media/ACR/Documents/Accreditation/MRI/LargePhantomInstructions.pdf). In particular, dual-echo TSE data were obtained with $TE_1 = 20$ ms, $TE_2 = 80$ ms, repetition time (TR) = 2000 ms, field-of-view (FOV) = 25 cm, 11 slices, 5-mm slice thickness with interslice gap of 5 mm, number of excitations (NEX) = 1, and matrix size of 256 × 256. Quantification of T_2^{eff} was determined by

$$T_2^{eff}(x,y,z) = \frac{TE_2 - TE_1}{\ln\left(\frac{S_1(x,y,z)}{S_2(x,y,z)}\right)} \quad (1)$$

where T_2^{eff} is the estimated effective T_2 in the voxel at coordinate (x, y, z), TE_1 and TE_2 are the TEs of the first and second MR image, respectively, and S_1 and S_2 are the MR signal intensity in the voxel at coordinate (x, y, z) at the two TEs, respectively. The mean value of T_2^{eff} was determined for the entire phantom at slice 6 using the standard ACR slice prescription, corresponding to a slice containing relatively homogeneous signal intensity and no internal geometric structures.

Patients

A total of 134 patients with gliomas who were evaluated using dual-echo TSE between 2000 and 2008 were retrospectively evaluated in this study. All patients gave informed written consent to be included in our institutional review board approved neuro-oncology database prior to this study. These 134 patients were broken into four groups for training and testing purposes: (i) 50 patients with various glioma grades used for training; (ii) 25 newly diagnosed glioblastoma patients treated with radiotherapy and no concurrent chemotherapy, none of which ever were exposed to bevacizumab; (iii) 35 newly diagnosed glioblastoma patients treated according to the current standard of care including radiotherapy with concurrent temozolomide (TMZ), followed by adjuvant TMZ; and 4) 24 recurrent glioblastoma patients treated with bevacizumab. Because this was a retrospective study, sample sizes were based solely on availability of data in patients that met the inclusion criteria outlined below.

Training set for defining NET. A total of 50 glioma patients with obvious NET who were evaluated using dual-echo TSE between 2000 and 2008 were retrospectively evaluated. Patients were selected so the training set contained tumors with a variety of WHO grades, histologic subtypes, and were at various stages of their disease. A total of 34 of 50 (68%) patients were male, approximately half the patients (26/50, 52%) were scanned on

Published OnlineFirst April 21, 2015; DOI: 10.1158/1078-0432.CCR-14-2862

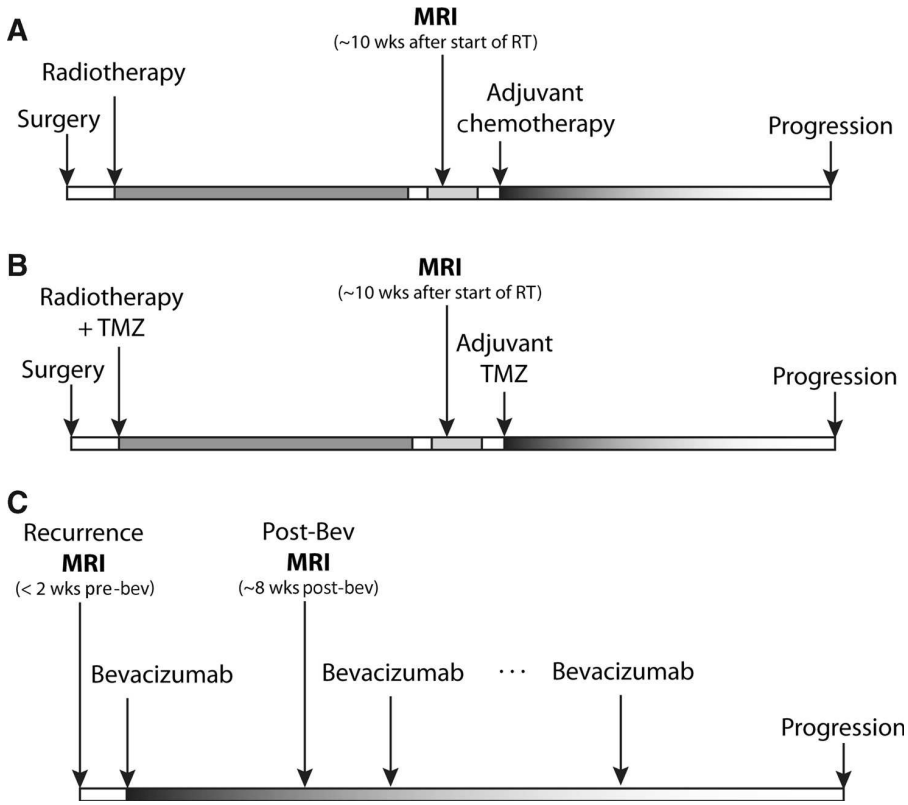

Figure 1.
Treatment paradigms for testing the prognostic and predictive utility of T_2^{eff}-defined NET volumes. A, newly diagnosed glioblastoma patients treated with radiotherapy were evaluated 10 weeks following the start of radiation. B, newly diagnosed glioblastoma patients treated with concurrent radiation and temozolomide therapy followed by adjuvant temozolomide were evaluated 10 weeks following concurrent radiation and temozolomide, prior to the start of adjuvant temozolomide. C, patients with recurrent glioblastoma treated with bevacizumab were evaluated before and after the first dose of bevacizumab therapy.

a 1.5T MR scanner, and the other half (24/50, 48%) was scanned on a 3T scanner. A total of 32 of 50 (64%) patients had recurrent tumors. Approximately 15 of 50 tumors (30%) were World Health Organization (WHO) grade II astrocytomas, 15 of 50 tumors (30%) were WHO III anaplastic astrocytoma (9/15) or oligodendrogliomas (6/15), and 20 of 50 (40%) were WHO IV glioblastomas. To estimate T_2^{eff} values in specific tissues, circular regions of interest (ROI) 1 cm in diameter were placed in areas of obvious normal-appearing white matter (NAWM), edema, NET, and necrosis on T_2-weighted images in these 50 patients. Regions of NET were defined as having a lower T_2 signal intensity compared with CSF, architectural distortion of the gray–white matter junction, or significant mass effect, whereas edematous tissue was defined as having a higher T_2 signal intensity approaching that of CSF, T_2 hyperintensity respecting the gray–white matter junction, no significant mass effect, and presence of "finger-like" projections of high-intensity T_2 signal within deep white matter, as defined previously by Pope and colleagues (17). The average T_2^{eff} for these regions were retained and used to define field strength–specific thresholds to accurately delineate NET from both edema and NAWM using ROC analysis.

Newly diagnosed glioblastoma patients treated with radiotherapy. A total of 25 newly diagnosed glioblastoma patients [average age, 53.2; range, 24–78 years old; average Karnofsky performance status (KPS), 83; range, 70–100; 16 of 25 were male (64%)] treated with 60 Gy intensity-modulated radiotherapy (IMRT) with no concurrent chemotherapy who were evaluated following completion of IMRT using dual-echo TSE between 2000 and 2008 were retrospectively evaluated (Fig. 1A). None of the 25 patients were ever treated with bevacizumab during their clinical history. All 25 patients were treated with adjuvant chemotherapies, including isotretinoin (Accutane; Roche Pharmaceuticals; 100 mg/m^2 orally for 21 consecutive days followed by 7 drug-free days), temozolomide (150 to 200 mg/m^2 i.v. or orally for 5 days of a 28-day cycle), lomustine (CCNU, Bristol-Myers Squibb; 110 mg/m^2 orally once every 6 weeks), or carboplatin (area under the plasma curve 4 mg/mL-min on day 1 of a 28-day cycle), until treatment failure.

Newly diagnosed glioblastoma patients treated with concurrent radiotherapy and temozolomide followed by adjuvant temozolomide. A total of 35 newly diagnosed glioblastoma patients [average age, 58; range, 27 to 77 years old; average KPS, 85; range, 70–100; 27/35 were male (77%)], treated concurrently with IMRT and temozolomide followed by adjuvant temozolomide (TMZ) who were evaluated following completion of concurrent IMRT and TMZ using dual-echo TSE between 2000 and 2008, were retrospectively evaluated (Fig. 1B). Patients were treated with 60Gy IMRT with concomitant TMZ (75 mg/m^2 orally or intravenously for 42 consecutive days) followed by adjuvant TMZ (150 mg/m^2 orally or intravenously for 5 consecutive days in the first 28-day cycle, followed by 200 mg/m^2 orally or intravenously for 5 consecutive days in the first 28-day cycle for a maximum of 6 cycles). Adjuvant TMZ was continued until disease progression, death, or completion of 6 cycles. A total of 8 of 35 patients (23%) were treated with bevacizumab during their clinical history, and 6 of the 8 patients were treated at first recurrence. Approximately 29 of

Published OnlineFirst April 21, 2015; DOI: 10.1158/1078-0432.CCR-14-2862

the 35 patients (83%) were treated with chemotherapy at first recurrence, including isotretinoin (Accutane, Roche Pharmaceuticals; 100 mg/m^2 orally for 21 consecutive days followed by 7 drug-free days, dose range across all patients = 160 to 200 mg; N = 9 patients), lomustine (CCNU, Bristol-Myers Squibb; 110 mg/m^2 orally once every 6 weeks, dose range across all patients = 150 to 210 mg; N = 17 patients), or carboplatin (area under the plasma curve 4 mg/mL-min on day 1 of a 28-day cycle; N = 3 patients).

Recurrent glioblastoma treated with bevacizumab. An independent sample of 24 patients with recurrent glioblastoma [average age, 56; range, 27–91 years old; average KPS, 82; range, 70–100; 12/24 were male (50%)] who failed IMRT and TMZ who also underwent evaluation at recurrence (baseline) and 2 to 4 weeks after the first administration of bevacizumab (10 mg/kg intravenously every 14 days) using dual-echo TSE between 2000 and 2008 were retrospectively evaluated (Fig. 1C). All patients were treated with bevacizumab every 14 days until disease progression or death.

Magnetic resonance imaging

Standard anatomical MR images including dual-echo TSE images for patients included in the training dataset were collected on one of the 1.5T or 3T MR scanners listed in Fig. 1. Standard anatomic images included an axial T1-weighted fast spin-echo sequence or magnetization-prepared rapid acquisition gradient-echo sequence (repetition time ms/TE ms/inversion time ms, 400–3,209/3.6–21.9/0–1,238; section thickness, 3–6.5 mm; intersection gap, 0–2.5 mm; number of signals acquired, one to two; matrix size, 176–512 × 256–512; and field of view, 24–25.6 cm) and a fluid-attenuated inversion-recovery sequence. In addition, axial T1-weighted images enhanced with gadopentetate dimeglumine (Magnevist; Berlex), 0.1 mmol/kg, and acquired shortly after contrast material injection, were matched to nonenhanced T1-weighted images obtained with similar sequence parameters. Dual-echo TSE images for the training dataset included both proton density/T2-weighted imaging pairs (e.g., TE_1 = 5–10 ms, TE_2 = 80–120 ms) or 2 sets of T2-weighted images (e.g., TE_1 = 80–120 ms, TE_2 = 160–200 ms). All therapeutic evaluations in this study were collected on a 1.5T MR scanner (Avanto or Sonata, Siemens Healthcare; Excite HDx or LX, GE Medical Systems) and all dual-echo TSE images had full brain coverage with TE_1 = 9–15 ms, TE_2 = 118–135 ms, TR = 4,000 ms, matrix size = 256 × 256, FOV = 240 mm, and slice thickness = 3 mm with no interslice gap.

Definition of disease progression

Progression was defined prospectively by the treating neuro-oncologists using a method consistent with the current RANO criteria (29). In particular, progression was defined if subsequent scans showed an increase in imaging-evaluable tumor (≥25% increase in the sum of enhancing lesions, new enhancing lesions >1 cm^2, an unequivocal qualitative increase in NET, or an unequivocal new area of noncontrast enhancing tumor). Patients were required to have stable or decreasing contrast agent dose before partial or complete response could be determined. In addition, patients requiring increased dosage of steroids in order to maintain neurologic function, even in the absence of worsening on anatomical images, were considered to be stable, but required early reevaluation. Patients who experienced significant neurologic decline were also declared to have progressed at the time of irreversible decline. Landmark PFS was therefore defined as being the number of days between the posttreatment MRI scan (e.g., post-radiotherapy or post-bevacizumab) and declared progression. Landmark OS was defined as the number of days between the posttreatment MRI scan to death.

Automated segmentation and quantification of NET burden

Multiple studies have demonstrated that the T_2 characteristics for NET fall between T_2 measurements of NAWM and edema (i.e., $T_2^{eff}{}_{NAWM} < T_2^{eff}{}_{tumor} < T_2^{eff}{}_{edema}$; 16–21). The particular thresholds used for tumor segmentation were determined empirically from the 50 glioma patients as per the experiment described above. After defining these thresholds, a 3-step automated procedure was performed to segment regions of NET from surrounding tissues (Supplementary Fig. SA): (i) First, the skull was stripped and all tissue with T_2^{eff} greater than the threshold to delineate tumor and NAWM were isolated, effectively removing NAWM and retain tumor, edema, and necrosis. (ii) Next, one image voxel surrounding these regions was eroded in order to remove tissues on the border of edema and NAWM, for example, where a partial volume voxel may have T_2^{eff} characteristics similar to tumor. A whole brain mask was then applied to confine all ROIs inside the brain. (iii) Finally, NET was segmented from regions of edema within the ROIs using the empirical thresholds defined previously and a cluster-based algorithm using a single voxel nearest-neighbor algorithm was used to isolate the largest contiguous clusters with T_2^{eff} values consistent with NET within the brain. Cluster sizes greater than 0.1 cc confluent with the primary enhancing lesion were retained for subsequent analyses. A single investigator confirmed adequate automatic segmentation, including verification that clusters were isolated in regions that could contain tumor.

Statistical analyses

Phantom measurements. To determine the stability of T_2^{eff} measurements in the ACR phantom over time, we examined the average coefficient of variance for 1.5T and 3T scanners independently over 3 years. A t test was used to compare average T_2^{eff} measurement values between 1.5T and 3T scanners.

Training data

For comparisons of T_2^{eff} measurements in various tissue types, a one-way ANOVA was used to examine T_2^{eff} measurements in NET across tumor grade, and a two-way ANOVA including interaction terms along with the Tukey test for multiple comparisons was used to examine differences in T_2^{eff} measurements across tissue types and field strengths. In addition, ROC analysis was used to determine the sensitivity and specificity for delineating various tissue types, including NET from edema and NET from NAWM for specific T_2^{eff} thresholds.

Newly diagnosed glioblastoma treated with radiotherapy. For newly diagnosed glioblastoma patients treated with radiation alone followed by adjuvant chemotherapy, ROC analysis was used to determine whether the volume of NET burden (selected from ROC analysis of training data) could stratify patients who progressed 6 months as well as those who expired within 9 months following completion of radiotherapy. Log-rank univariate analysis applied to Kaplan–Meier data was used to

Published OnlineFirst April 21, 2015; DOI: 10.1158/1078-0432.CCR-14-2862

determine whether patients with a large NET burden (from ROC analysis) had significantly shorter PFS and OS. A Cox multivariate proportional hazards model was then used to determine whether NET volume quantified using T_2^{eff} was an independent predictor of PFS and OS after including covariates including patient age and KPS.

Newly diagnosed glioblastoma treated with concurrent radiotherapy and temozolomide followed by adjuvant temozolomide. For newly diagnosed glioblastoma patients treated with concurrent radiation and temozolomide followed by adjuvant temozolomide, ROC analysis was used to determine whether the volume of NET burden (selected from ROC analysis of training data) could stratify patients who progressed 6 months as well as those who expired within 9 months following completion of radiotherapy. Log-rank univariate analysis applied to Kaplan–Meier data was used to determine whether patients with a large NET burden (from ROC analysis) had significantly shorter PFS and OS. A Cox multivariate proportional hazards model was then used to confirm whether NET burden quantified using T_2^{eff} was an independent predictor of PFS and OS after including covariates including patient age and KPS.

Recurrent glioblastoma treated with bevacizumab. For recurrent glioblastoma patients treated with bevacizumab, ROC analysis was used to determine whether the volume of NET burden (selected from ROC analysis of training data) could stratify patients who progressed 6 months as well as those who expired within 9 months following start of bevacizumab. Log-rank univariate analysis applied to Kaplan–Meier data was used to determine whether small changes in NET burden (from ROC analysis) had significantly shorter PFS and OS. A Cox multivariate proportional hazards model was then used to confirm that change in NET burden before and after bevacizumab was an independent predictor of PFS and OS after including covariates including patient age and KPS.

Results

Evaluations of the ACR phantoms using the dual-echo TSE sequence showed reasonable stability over time, averaging a coefficient of variance of approximately 3.4% for 3T scanners and 4.5% for 1.5T scanners when evaluated over the last 3 years. The coefficient of variance of T_2^{eff} measurements across the 3T scanners was 3.1% and across all 1.5T scanners was 4.5%, suggesting long-term stability was similar to the stability across scanners at a single time point. T_2^{eff} measurements on 3T MR scanners were significantly lower than 1.5T scanners (Fig. 2; *t* test, $P < 0.0001$; T_2^{eff} in 3T = 79.3 ± 2.5 ms vs. 1.5T = 98.8 ± 4.4 ms), confirming the expected decrease in T_2 relaxation times for increasing magnetic field strength.

A total of 50 patients with various tumor grades containing regions of obvious NET as training data for delineation of NET from other tissues based on specific T_2^{eff} measurements. In general, T_2^{eff} maps appeared relatively similar across field strengths (Fig. 3), with areas of obvious edema or necrosis showing a higher $T2^{eff}$, areas of NAWM showing the lowest T_2^{eff}, and regions of suspected NET adjacent or contiguous with enhancing tumor showing T_2^{eff} measurements between edema and NAWM. No differences in T_2^{eff} measurements were observed in NET components across tumor grade (ANOVA, $P = 0.8678$).

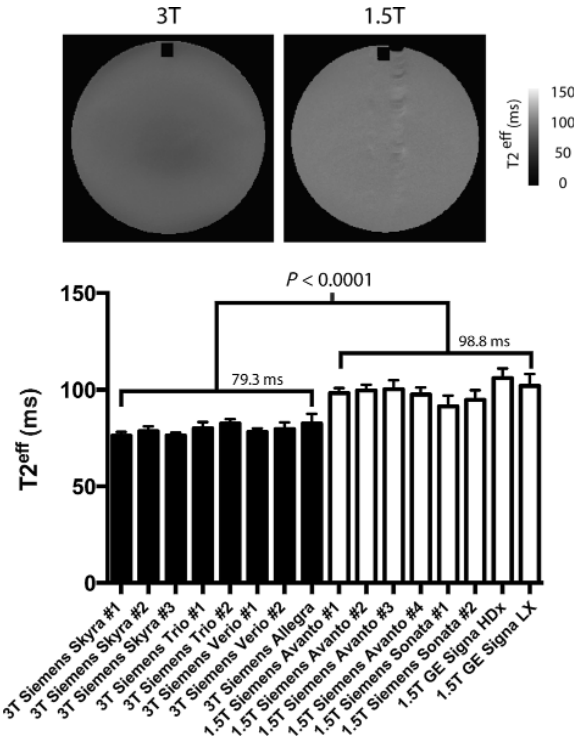

Figure 2.
Dual-echo TSE estimates of T_2^{eff} obtained in an American College of Radiology (ACR) phantom for 16 different MRI scanners. Results show a significant difference in T_2^{eff} measurements in 3T (mean = 79.3 ms) versus 1.5T (mean = 98.8 ms) scanners.

Measurement of T_2^{eff} in the various tissues confirmed this observation (Fig. 4A). A two-way ANOVA showed a significant difference between tissue types ($P < 0.0001$), field strength ($P < 0.0001$), and the interaction between tissue types and field strength ($P < 0.0001$). Multiple comparisons tests showed significant differences between T_2^{eff} values for each tissue type within both 1.5T and 3T data (Tukey test, $P < 0.01$ for all comparisons between tissue types within 1.5T and 3T). Within each tissue type, T_2^{eff} values were significantly different across field strengths in edema and necrotic tissues ($P < 0.01$), but no difference was observed between T_2^{eff} values within NAWM or tumor. This suggests that a single threshold may be used across field strengths to differentiate NAWM and tumor from other tissues.

ROC analysis suggested that T_2^{eff} could significantly stratify NET from edema (Fig. 4B; 1.5T: ROC AUC = 0.9000 ± 0.0219, $P < 0.0001$; 3T: AUC = 0.9773 ± 0.01199, $P < 0.0001$). A threshold of 250 ms could be used to stratify NET from edema with a sensitivity of 91% and specificity of 71% at 1.5T, and a sensitivity of 100% and specificity of 65% at 3T. ROC analysis suggested that $T2^{eff}$ could also stratify NET from NAWM (Fig. 4B; 1.5T: AUC = 0.9934 ± 0.0043, $P < 0.0001$; 3T: AUC = 0.9974 ± 0.0030, $P < 0.0001$). A threshold of 125 ms could be used to stratify NET from NAWM with a sensitivity of sensitivity of 96% and specificity of 97% at 1.5T, and 94% sensitivity and 97% specificity at 3T. Thus, we propose using a range of T_2^{eff} values between 125 ms < T_2^{eff} < 250 ms, on both 1.5T and 3T MR scanners, to objectively define NET for the

Published OnlineFirst April 21, 2015; DOI: 10.1158/1078-0432.CCR-14-2862

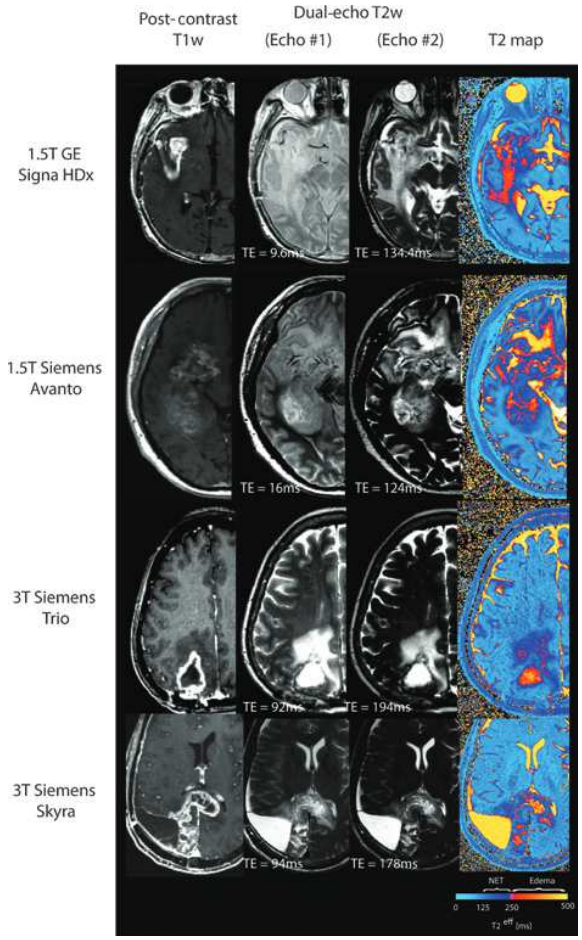

Figure 3.
Postcontrast T1-weighted images, dual-echo TSE images, and T_2^{eff} maps of five patients with glioblastoma scanned on different MRI scanners with slightly different acquisition parameters.

purpose of tumor burden quantification. Figure 4C shows a patient with a recurrent glioblastoma containing a large, well-circumscribed NET appearing as slightly T_2 hyperintense on T2-weighted images at 3T. T_2^{eff} maps clearly show that this NET falls largely within the defined range of 125 ms < T_2^{eff} < 250 ms. Conversely, Fig. 4D also shows a patient with recurrent glioblastoma scanned at 3T with a large extent of edematous tissue, as demonstrated by the "finger-like" extensions of very bright T_2 hyperintensity on T_2-weighted images. Consistent with these qualitative observations, most of this lesion had elevated T_2^{eff} within the range associated with edema. In addition, an area near the right insula with relatively lower signal intensity on T_2 -weighted images (red arrow) also containing contrast enhancement (not shown) appears to have T_2^{eff} values within the range defined as NET. MR spectroscopic imaging (MRSI) also confirmed that areas defined as NET on T_2^{eff} maps were often associated with increased choline concentration in a subset of patients (Fig. 4E and F), suggestive of freely mobile phosphocholine from the cell membrane turnover in actively proliferating tumor cells.

Using 125 ms < T_2^{eff} < 250 ms to objectively define NET, we aimed to test whether the volume of NET burden following radiotherapy alone was a prognostic predictor in patients with newly diagnosed glioblastoma (Fig. 5A–C). The average volume of NET burden for the cohort was estimated at 39.6 cc ± 7.2 cc (SEM) and a range from 0.3 cc to 119 cc. Results suggest that NET volume measured following radiotherapy could identify patients who progressed within 6 months following completion of radiotherapy (Fig. 5A; ROC AUC = 0.8590 ± 0.07248, P = 0.002) as well as those who expired within 9 months following completion of radiotherapy (Fig. 5A; ROC AUC = 0.8467 ± 0.08341, P = 0.004). A threshold of 32 cc, the median volume of NET, was shown to have a sensitivity of 69% and specificity of 79% for identifying patients who progressed within 6 months of radiotherapy and a sensitivity of 70% and specificity of 90% for identifying patients who expired within 9 months of completion of radiotherapy. Patients with NET volumes larger than 32 cc had a significantly shorter PFS (Fig. 5B; log-rank, P = 0.0013, HR = 2.219, median survival for high vs. low NET volume = 132 vs. 294 days) and OS (Fig. 5C; log-rank, P = 0.0071, HR = 2.982, median OS for high vs. low NET volume = 228 vs. 681 days). Cox multivariate regression including clinical covariates of both age and KPS confirmed that NET volume after radiotherapy was a significant predictor of subsequent PFS (Table 1; Cox proportional hazards, P = 0.0216, HR = 2.8410 ± 1.5756 SEM) and OS (Cox proportional hazards, P = 0.0014, HR = 5.3475 ± 1.6925 SEM). Age at diagnosis was also a prognostic factor in patients with newly diagnosed glioblastoma treated with radiotherapy (age: PFS, P = 0.0132, HR = 1.0461 ± 1.0184 SEM; OS, P = 0.0028, HR = 1.0631 ± 1.0207), but KPS was not predictive (KPS: PFS, P = 0.4433; OS, P = 0.1526).

Next, we aimed to test whether the volume of NET burden following radiotherapy combined with temozolomide followed by adjuvant temozolomide was a prognostic predictor in patients with newly diagnosed glioblastoma (Fig. 5D and F). The average volume of NET burden for the cohort was estimated at 34.1 cc ± 4.7 cc (SEM) and a range from 0.6 cc to 122 cc. Results suggest that NET volume evaluated following combined radiotherapy and temozolomide could not identify patients who progressed within 6 months following completion of radiochemotherapy (Fig. 5D; ROC AUC = 0.5906 ± 0.0963, P = 0.3850) or patients at risk for expiring within 9 months following completion of radiochemotherapy (Fig. 5D; ROC AUC = 0.6733 ± 0.0925, P = 0.08304). Patients with NET volumes larger than the median NET volume of 23 cc for this cohort following radiochemotherapy were at significantly higher risk for shorter PFS (Fig. 5E; log-rank, P = 0.035, HR = 2.217, median PFS for high vs. low NET volume = 67 vs. 149 days) and OS (Fig. 5F; log-rank, P = 0.0335, HR = 1.1660, median OS for high vs. low NET volume = 181 vs. 301 days). Cox multivariate regression including clinical covariates confirmed this trend (Table 2), showing that NET volume following completion of radiochemotherapy was a significant independent predictor of both PFS (Cox proportional hazards, P = 0.0323, HR = 2.3708 ± 1.4690 SEM) and OS (Cox proportional hazards, P = 0.0004, HR = 2.7907 ± .5173 SEM). Age and KPS at diagnosis were not prognostic factors for PFS or OS in newly diagnosed glioblastoma patients treated with radiochemotherapy (age: PFS, P = 0.7711, OS, P = 0.3520; KPS: PFS, P = 0.2745; OS, P = 0.2450).

Published OnlineFirst April 21, 2015; DOI: 10.1158/1078-0432.CCR-14-2862

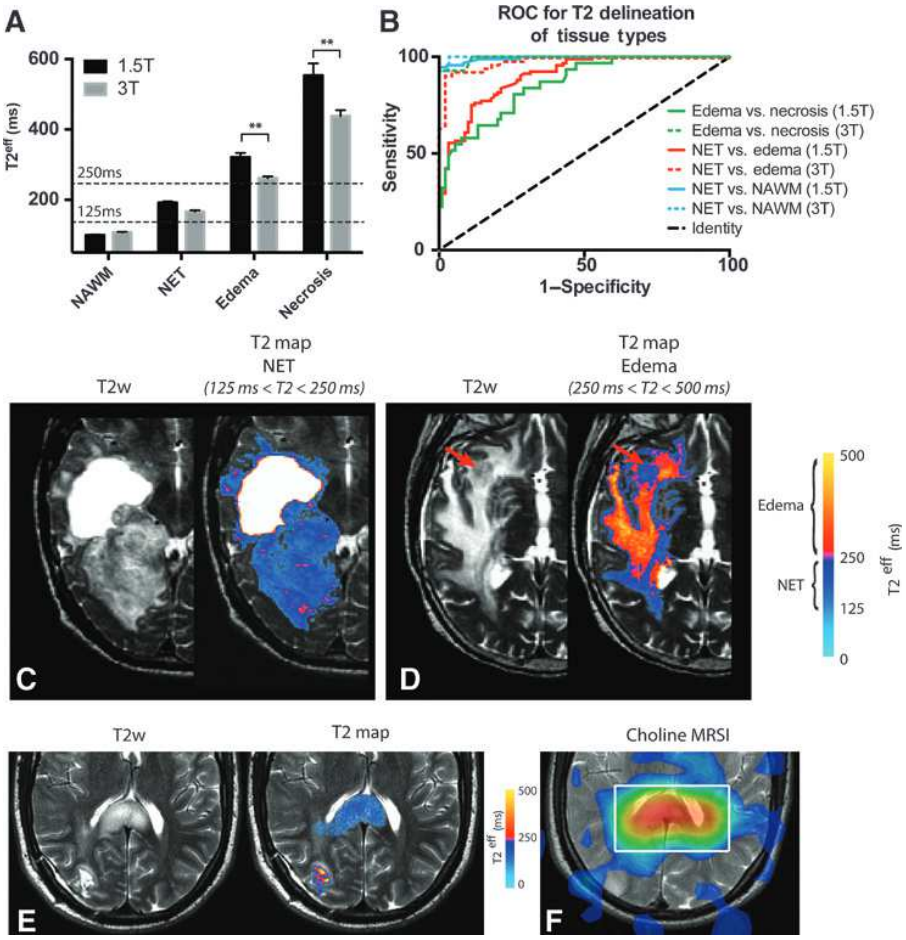

Figure 4.
Training data used for delineating NET from other tissues. A, mean T_2^{eff} measurements for normal-appearing white matter (NAWM), NET, edema, and necrosis for both 1.5T and 3T. Error bars represent SEM across all 25 patients scanned at either 1.5T or 3T. B, ROC curves showing delineation between edema and necrosis, NET and edema, and NET and NAWM for both 1.5T and 3T. C, an example of a patient with glioblastoma with a l arge NET mass as evidenced by the well-circumscribed, slightly T_2 -hyperintense lesion adjacent to the resection cavity. T_2^{eff} maps show that this mass falls within the range defined as NET in this study (125 ms < T_2^{eff} < 250 ms). D, an example of a glioblastoma patient with a large T_2-hyperintense lesion consistent with a mostly edematous mass as evidenced by the high T_2 -hyperintense signal and "finger-like" white matter extensions. An area consistent with T_2^{eff}-defined NET is shown (red arrow), which also is colocalized to the area of contrast enhancement (not shown). E, a patient with a low-grade glioma shown to have an NET mass within the splenium of the corpus callosum on T_2^{eff} maps. F, MRSI choline metabolic maps show high choline concentration in this area, consistent with metabolically active tumor.

Finally, we tested whether early NET response measured as the change in NET volume before and after bevacizumab therapy could be used to predict survival in patients with recurrent glioblastoma (Fig. 5G and I). The average volume of NET burden for the cohort prior to and after bevacizumab therapy was estimated at 30.3 cc ± 3.7 cc (SEM) and 15.8 cc ± 3.5 cc (SEM), respectively. The average change in NET volume was −14.5 cc ± 2.7 cc (SEM). Results demonstrated that changes in NET volume before and after bevacizumab therapy could be used to identify patients who progressed within 6 months of completion of the first dose of bevacizumab (Fig. 5G; ROC AUC = 0.7786 ± 0.0967, $P = 0.022$), as well as patients who expired within 9 months of completion of the first dose of bevacizumab (Fig. 5G; ROC AUC = 0.8681 ± 0.07399, $P = 0.002$). A decrease in NET volume greater than 50% was found to have a sensitivity of 70% and specificity of 71% for identifying patients that will progress within 6 months of starting bevacizumab therapy, along with a sensitivity of 83% and specificity of 67% for identifying patients that will expire within 9 months of starting bevacizumab therapy. Patients showing a "response," or more than 50% decrease in NET volume after bevacizumab therapy, had a significantly longer PFS (Fig. 5H; log-rank, $P = 0.00070$, HR = 2.565, median PFS for responders vs. nonresponders = 215 vs. 84 days) and OS (Fig. 5I; log-rank, $P = 0.0105$, HR = 2.00, median OS for responders vs. nonresponders = 375 vs. 187 days). Cox multivariate regression confirmed this observation (Table 3), showing longer PFS (Cox proportional hazards, $P = 0.0071$, HR = 1.0189 ± 1.0070) and OS (Cox proportional hazards, $P = 0.0377$, HR = 1.0122 ± 1.0058) in patients demonstrating more than a 50% decrease in NET volume after the first dose of bevacizumab. Both age and KPS were not significant prognostic factors for recurrent glioblastoma patients treated with bevacizumab (age: PFS, $P = 0.1090$, OS, $P = 0.1220$; KPS: PFS, $P = 0.5283$, OS, $P = 0.7142$).

Discussion

Results from this study support the hypothesis that T_2 maps quickly obtained using dual-echo TSE images can be used to objectively define and quantify NET burden. Results support the concept that quantification of NET is clinically meaningful and prognostic, as demonstrated both by the prognostic significance of NET tumor burden following radiotherapy with or without temozolomide as well as the change in NET volume as a simple response measure during bevacizumab therapy in recurrent glioblastoma. This is a particularly timely question as this concept has come into serious debate recently (9). In particular, studies have suggested limited value of including challenging and costly qualitative assessment of NET response when evaluating drug efficacy,

Published OnlineFirst April 21, 2015; DOI: 10.1158/1078-0432.CCR-14-2862

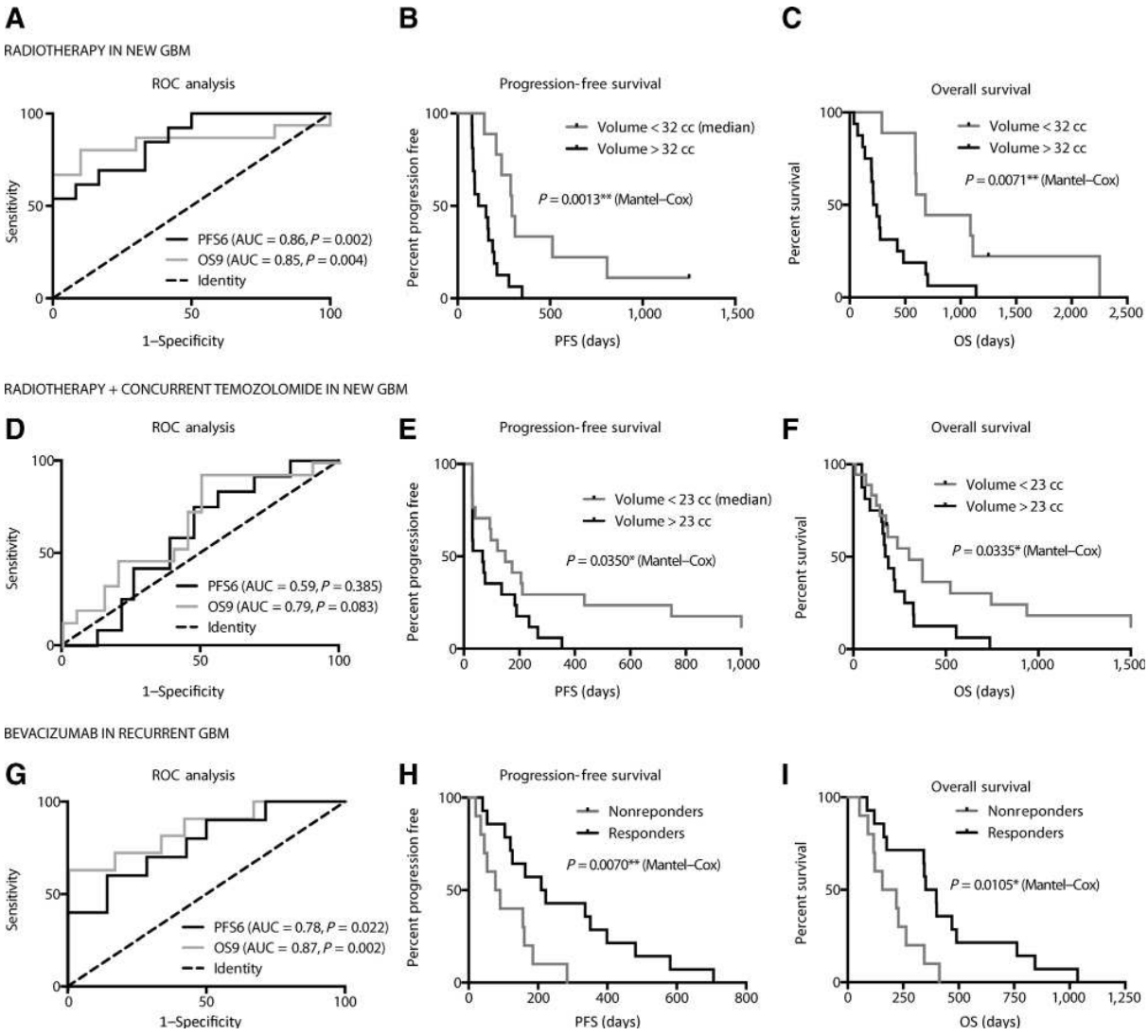

Figure 5.
ROC curves, PFS, and OS using T_2^{eff}-defined NET volumes in newly diagnosed glioblastoma patients treated with radiotherapy or radiotherapy and concurrent temozolomide, and recurrent glioblastoma treated with bevacizumab. A, ROC analysis performed using NET volume estimates following radiotherapy to predict 6-month PFS (PFS6) and 9-month OS (OS9). B, Kaplan–Meier curves showing that the median volume of NET (32 cc) could stratify long-term and short-term PFS in newly diagnosed glioblastoma patients treated with radiotherapy (P = 0.0013). C, Kaplan–Meier curves showing the median volume of NET (32 cc) could also stratify long-term and short-term OS in newly diagnosed glioblastoma patients treated with radiotherapy (P = 0.0071). D, ROC analysis performed using NET volume estimates following concurrent radiotherapy and temozolomide to predict PFS6 and OS9. Results did not show statistical significance for either PFS6 or OS9 in this patient cohort. E, Kaplan–Meier curves illustrating that the median volume of NET (23 cc) could stratify long- and short-term PFS in newly diagnosed glioblastoma patients treated with concurrent radiotherapy and temozolomide followed by adjuvant temozolomide (P = 0.0350). F, Kaplan–Meier curves showing that median NET volume (23 cc) could stratify long-term and short-term OS (P = 0.0335). G, ROC analysis performed using the change in NET volume before and after bevacizumab treatment in recurrent glioblastoma to predict PFS6 and OS9. H, Kaplan–Meier curves demonstrating that recurrent glioblastoma patients with more than 50% decrease in NET volume following bevacizumab therapy ("responders") have a longer PFS compared with patients demonstrating less than a 50% decrease in NET volume ("nonresponders"; P = 0.0070). I, Kaplan–Meier curves showing that recurrent glioblastoma patients showing "response" to bevacizumab on NET have a significantly lower OS compared with "nonresponders" (P = 0.0105).

as response rates and PFS estimates seem comparable with and without the use of NET assessment (1) and in most instances, NET progression results in contrast enhancing tumor progression by the subsequent follow-up examination (30). In addition, recent results from ACRIN 6677/RTOG 0625, a prospective, randomized, phase II multicenter trial comparing bevacizumab with either irinotecan or temozolomide in recurrent glioblastoma, demonstrated that response rate of contrast enhancing tumor was predictive of OS, whereas NET progression rates did not predict OS (31). Regardless, a large proportion of patients are

Published OnlineFirst April 21, 2015; DOI: 10.1158/1078-0432.CCR-14-2862

Table 1. Cox proportional hazards model results for newly diagnosed glioblastoma treated with radiotherapy

	PFS		OS	
	HR	P	HR	P
Age	1.0461 ± 1.0184	0.0132	1.0631 ± 1.0207	0.0028
KPS	1.0184 ± 1.0240	0.4433	0.9624 ± 1.0271	0.1526
T_2^{eff} defined NET >32 cc	2.8410 ± 1.5756	0.0216	5.3475 ± 1.6925	0.0014

NOTE: Error bars represent ± SEM.

Table 3. Cox proportional hazards model results for recurrent glioblastoma treated with bevacizumab

	PFS		OS	
	HR	P	HR	P
Age	0.9703 ± 1.0190	0.1090	0.9746 ± 1.0168	0.1220
KPS	0.9840 ± 1.0259	0.5283	0.9909 ± 1.0254	0.7142
Reduction in NET > 50%	1.0189 ± 1.0070	0.0071	1.0122 ± 1.0058	0.0377

NOTE: Error bars represent ± SEM.

expected to experience NET progression prior to changes in contrast enhancement and the vast majority of low-grade gliomas do not have contrast enhancement, reinforcing the need for an objective definition of nonehancing tumor using quantitative MRI.

Although ROC analysis demonstrated that NET burden could be used to quickly identify newly diagnosed glioblastomas at high risk for progressing by 6 months or expiring before 9 months when treated with radiotherapy alone, this same time point was of limited predictive value in patients treated with radiotherapy and concurrent temozolomide, the current standard of care for newly diagnosed glioblastoma. These results may be influenced by other molecular characteristics of the tumor, such as MGMT promoter methylation status or gene expression subtype. Future studies with larger patient cohorts are necessary to identify the roles of these additional prognostic factors.

Results demonstrate that T_2^{eff} measurements using dual-echo TSE are relatively stable, varying approximately 3% to 5% over time and across scanners of similar field strength when evaluated in phantoms. This is consistent with previous reports showing variation in normal tissues of between 5% and 15% (23, 32, 33), on par with errors due to the specific pulse sequence and vendor specific errors (34). T_2 estimation using dual-echo TSE techniques, however, has been shown to slightly overestimate T_2 by as much as 10% (26, 35–37). This bias in T_2 estimation arises from multiple sources, including the use of only a few echoes for estimation, spurious signals from stimulated echoes, radiofrequency pulse imperfections, and different phase encoding profile orders (26, 38, 39). Despite this inaccuracy, T_2 mapping using dual-echo TSE acquisition has proven very useful for identification of various pathologies, including Alzheimer's and other neurodegenerative diseases (23, 36, 40, 41). Techniques to overcome this slight bias have been developed (38), although they remain relatively cumbersome to implement and are not often used in clinical practice. Importantly, the Alzheimer's disease neuroimaging initiative chose to implemented dual-echo T_2-weighted TSE for estimation of pathology-specific changes in quantitative T_2; thus, a standardized dual-echo TSE sequence is openly available from all major MRI vendors, which further supports the view of using dual-echo T2-weighted TSE to quantify "effective T_2" (T_2^{eff}) for use in objectively defining NET burden within clinically realizable scan times.

Table 2. Cox proportional hazards model results for newly diagnosed glioblastoma treated with concurrent radiotherapy and temozolomide

	PFS		OS	
	HR	P	HR	P
Age	0.9939 ± 1.0211	0.7711	1.0251 ± 1.0270	0.3520
KPS	1.0227 ± 1.0207	0.2745	1.0270 ± 1.0232	0.2450
T_2^{eff} defined NET >23 cc	2.3708 ± 1.4969	0.0323	2.7907 ± 1.5173	0.0138

NOTE: Error bars represent ± SEM.

It is important to point out that there remains significant overlap between T_2^{eff} measurements within regions believed to contain mixtures of edema and NET, thus quantification of NET burden in this study may not be completely accurate. During the training phase, we chose to specifically identify regions containing obvious, pure NET with little partial volume contamination from edema or necrosis. It is both conceivable and highly likely that some regions classified as edema and not included in the quantification of NET burden contain active tumor, whereas some regions classified as NET may in fact contain substantial proportions of edema. Future studies aimed at histologic validation should be performed in order to further aid in defining NET burden using T_2^{eff} measurements.

Additional considerations and study limitations should also be addressed. For example, white matter changes after radiotherapy may have confounded our interpretation of various tissue types; however, we strategically included recurrent glioma patients in our training cohort in order to provide a more robust range of T2 values that might include treatment-related changes. Finally, this study lacks separate, independent validation of the primary findings. Future studies aimed at independent validation in a randomized, clinical trial, along with comparison to other imaging biomarkers, is warranted in order to establish effective T_2 maps as a surrogate for quantifying NET burden in patients with gliomas.

Conclusion

Dual-echo TSE can be used to objectively define NET burden for use in brain tumor characterization, prognosis, and response assessment. T_2^{eff} measurements obtained using dual-echo TSE has relatively low variability, is feasible at both 1.5T and 3T, and can be used to predict response and survival in patients with gliomas.

Disclosure of Potential Conflicts of Interest

B.M. Ellingson reports receiving commercial research grants from Roche/Genentech and Siemens Healthcare, and reports receiving speakers bureau honoraria from and is a consultant/advisory board member for Roche/Genentech. A. Lai reports receiving other research grants from Roche and Takeda, and is a consultant/advisory board member for Novocure and Roche. No potential conflicts of interest were disclosed by the other authors.

Authors' Contributions

Conception and design: B.M. Ellingson, A. Lai, W.B. Pope, T.F. Cloughesy
Development of methodology: B.M. Ellingson, W.B. Pope
Acquisition of data (provided animals, acquired and managed patients, provided facilities, etc.): B.M. Ellingson, A. Lai, P.L. Nghiemphu, T.F. Cloughesy
Analysis and interpretation of data (e.g., statistical analysis, biostatistics, computational analysis): B.M. Ellingson, A. Lai, W.B. Pope, T.F. Cloughesy

Published OnlineFirst April 21, 2015; DOI: 10.1158/1078-0432.CCR-14-2862

Writing, review, and/or revision of the manuscript: B.M. Ellingson, A. Lai, H.N. Nguyen, P.L. Nghiemphu, W.B. Pope, T.F. Cloughesy
Administrative, technical, or material support (i.e., reporting or organizing data, constructing databases): B.M. Ellingson, H.N. Nguyen
Study supervision: B.M. Ellingson, T.F. Cloughesy

Grant Support

This work was supported by the National Brain Tumor Society Research Grant (B.M. Ellingson and T.F. Cloughesy), NIH/NCI 1 R21 CA167354-01 (B.M. Ellingson), UCLA Institute for Molecular Medicine Seed Grant (B.M. Ellingson), UCLA Radiology Exploratory Research Grant (B.M. Ellingson), University of California Cancer Research Coordinating Committee Grant (B.M. Ellingson), ACRIN Young Investigator Initiative Grant (B.M. Ellingson), Art of the Brain (T.F. Cloughesy), Ziering Family Foundation in memory of Sigi Ziering (T.F. Cloughesy), Singleton Family Foundation (T.F. Cloughesy), Clarance Klein Fund for Neuro-Oncology (T.F. Cloughesy), National Institute of Health National Institute of General Medical Sciences training grant (GM08042), and the University of California Los Angeles Medical Scientist Training Program.

The costs of publication of this article were defrayed in part by the payment of page charges. This article must therefore be hereby marked *advertisement* in accordance with 18 U.S.C. Section 1734 solely to indicate this fact.

Received November 4, 2014; revised March 18, 2015; accepted April 8, 2015; published OnlineFirst April 21, 2015.

References

1. Gallego Perez-Larraya J, Lahutte M, Petrirena G, Reyes-Botero G, Gonzalez-Aguilar A, Houillier C, et al. Response assessment in recurrent glioblastoma treated with irinotecan-bevacizumab: comparative analysis of the Macdonald, RECIST, RANO, and RECIST + F criteria. Neuro Oncol 2012;14:667–73.
2. Nowosielski M, Wiestler B, Goebel G, Hutterer M, Schlemmer HP, Stockhammer G, et al. Progression types after antiangiogenic therapy are related to outcome in recurrent glioblastoma. Neurology 2014;82:1684–92.
3. Kelly PJ, Daumas-Duport C, Scheithauer BW, Kall BA, Kispert DB. Stereotactic histologic correlations of computed tomography- and magnetic resonance imaging-defined abnormalities in patients with glial neoplasms. Mayo Clin Proc 1987;62:450–9.
4. Kelly PJ, Daumas-Duport C, Kispert DB, Kall BA, Scheithauer BW, Illig JJ. Imaging-based stereotaxic serial biopsies in untreated intracranial glial neoplasms. J Neurosurg 1987;66:865–74.
5. Ellingson BM, Lai A, Harris RJ, Selfridge JM, Yong WH, Das K, et al. Probabilistic radiographic atlas of glioblastoma phenotypes. Am J Neuroradiol 2013;34:533–40.
6. Chamberlain MC. Radiographic patterns of relapse in glioblastoma. J Neurooncol 2011;101:319–23.
7. Jain RK, di Tomaso E, Duda DG, Loeffler JS, Sorensen AG, Batchelor TT. Angiogenesis in brain tumours. Nat Rev Neurosci 2007;8:610–22.
8. Wen PY, Cloughesy TF, Ellingson BM, Reardon DA, Fine HA, Abrey L, et al. Report of the jumpstarting brain tumor drug development coalition and FDA clinical trials neuroimaging endpoint workshop (January 30, 2014, Bethesda MD). Neuro Oncol 2014;16Suppl 7:vii36–47.
9. Ellingson BM, Wen PY, van den Bent MJ, Cloughesy TF. Pros and cons of current brain tumor imaging. Neuro Oncol 2014;16 Suppl 7:vii2–11.
10. Damadian R. Tumor detection by nuclear magnetic resonance. Science 1971;171:1151–3.
11. Weisman ID, Bennett LH, Maxwell LR Sr, Woods MW, Burk D. Recognition of cancer in vivo by nuclear magnetic resonance. Science 1972;178:1288–90.
12. Hazelwood CF, Chang DC, Medina D, Cleveland G, Nichols BL. Distinction between the preneoplastic and neoplastic state of murine mammary glands. Proc Natl Acad Sci U S A 1972;69:1478–80.
13. Hollis DP, Economou JS, Parks LC, Eggleston JC, Saryan LA, Czeister JL. Nuclear magnetic resonance studies of several experimental and human malignant tumors. Cancer Res 1973;33:2156–60.
14. Inch WR, McCredie JA, Knispel RR, Thompson RT, Pintar MM. Water content and proton spin relaxation time for neoplastic and non-neoplastic tissues from mice and humans. J Natl Cancer Inst 1974;52:353–6.
15. Hazlewood CF, Cleveland G, Medina D. Relationship between hydration and proton nuclear magnetic resonance relaxation times in tissues of tumor-bearing and non-tumor-bearing mice: implications for cancer detection. J Natl Cancer Inst 1974;52:1849–53.
16. Hoehn-Berlage M, Tolxdorff T, Bockhorst K, Okada Y, Ernestus RI. In vivo NMR T2 relaxation of experimental brain tumors in the cat: a multiparameter tissue characterization. Magn Reson Imaging 1992;10:935–47.
17. Pope WB, Sayre J, Perlina A, Villablanca JP, Mischel PS, Cloughesy TF. MR imaging correlates of survival in patients with high-grade gliomas. Am J Neuroradiol 2005;26:2466–74.
18. Eis M, Els T, Hoehn-Berlage M. High resolution quantitative relaxation and diffusion MRI of three different experimental brain tumors in rat. Magn Reson Med 1995;34:835–44.
19. Oh J, Cha S, Aiken AH, Han ET, Crane JC, Stainsby JA, et al. Quantitative apparent diffusion coefficients and T2 relaxation times in characterizing contrast enhancing brain tumors and regions of peritumoral edema. J Magn Reson Imaging 2005;21:701–8.
20. Schad LR, Brix G, Zuna I, Harle W, Lorenz WJ, Semmler W. Multiexponential proton spin-spin relaxation in MR imaging of human brain tumors. J Comput Assist Tomogr 1989;13:577–87.
21. Komiyama M, Yagura H, Baba M, Yasui T, Hakuba A, Nishimura S, et al. MR imaging: possibility of tissue characterization of brain tumors using T1 and T2 values. Am J Neuroradiol 1987;8:65–70.
22. Melki PS, Mulkern RV, Panych LP, Jolesz FA. Comparing the FAISE method with conventional dual-echo sequences. J Magn Reson Imaging 1991;1:319–26.
23. Landman BA, Huang AJ, Gifford A, Vikram DS, Lim IA, Farrell JA, et al. Multi-parametric neuroimaging reproducibility: a 3-T resource study. Neuroimage 2011;54:2854–66.
24. Ceccarelli A, Rocca MA, Perego E, Moiola L, Ghezzi A, Martinelli V, et al. Deep grey matter T2 hypo-intensity in patients with paediatric multiple sclerosis. Mult Scler 2011;17:702–7.
25. Chan I, Wells W 3rd, Mulkern RV, Haker S, Zhang J, Zou KH, et al. Detection of prostate cancer by integration of line-scan diffusion, T2-mapping and T2-weighted magnetic resonance imaging; a multichannel statistical classifier. Med Phys 2003;30:2390–8.
26. Leppert IR, Almli CR, McKinstry RC, Mulkern RV, Pierpaoli C, Rivkin MJ, et al. T(2) relaxometry of normal pediatric brain development. J Magn Reson Imaging 2009;29:258–67.
27. Okujava M, Schulz R, Ebner A, Woermann FG. Measurement of temporal lobe T2 relaxation times using a routine diagnostic MR imaging protocol in epilepsy. Epilepsy Res 2002;48:131–42.
28. Quaia E, Toffanin R, Guglielmi G, Ukmar M, Rossi A, Martinelli B, et al. Fast T2 mapping of the patellar articular cartilage with gradient and spin-echo magnetic resonance imaging at 1.5 T: validation and initial clinical experience in patients with osteoarthritis. Skeletal Radiol 2008;37:511–7.
29. Wen PY, Macdonald DR, Reardon DA, Cloughesy TF, Sorensen AG, Galanis E, et al. Updated response assessment criteria for high-grade gliomas: response assessment in neuro-oncology working group. J Clin Oncol 2010;28:1963–72.
30. Radbruch A, Lutz K, Wiestler B, Baumer P, Heiland S, Wick W, et al. Relevance of T2 signal changes in the assessment of progression of glioblastoma according to the Response Assessment in Neurooncology criteria. Neuro Oncol 2012;14:222–9.
31. Huang RY, Rahman R, Pope WB, Ellingson BM, Anderson KS, Felten SJ, et al. Validation of RANO criteria: contribution of T2/FLAIR assessment in patients with recurrent glioblastoma treated with bevacizumab. ASCO Annual Meeting; 2014; Chicago, IL; 2014. p. abstr 2007.
32. Jansen JF, Kooi ME, Kessels AG, Nicolay K, Backes WH. Reproducibility of quantitative cerebral T2 relaxivity, diffusion tensor imaging, and 1H magnetic resonance spectroscopy at 3T. Proc Intl Soc Mag Reson Med 2005;15:790.
33. Jansen JF, Kooi ME, Kessels AG, Nicolay K, Backes WH. Reproducibility of quantitative cerebral T2 relaxometry, diffusion tensor imaging, and

1H magnetic resonance spectroscopy at 3.0 Tesla. Invest Radiol 2007; 42:327–37.
34. Bauer CM, Jara H, Killiany R, Alzheimer's Disease Neuroimaging I. Whole brain quantitative T2 MRI across multiple scanners with dual echo FSE: applications to AD, MCI, and normal aging. Neuroimage 2010;52:508–14.
35. Roebuck JR, Haker SJ, Mitsouras D, Rybicki FJ, Tempany CM, Mulkern RV. Carr-Purcell-Meiboom-Gill imaging of prostate cancer: quantitative T2 values for cancer discrimination. Magn Reson Imaging 2009;27: 497–502.
36. Giri S, Chung YC, Merchant A, Mihai G, Rajagopalan S, Raman SV, et al. T2 quantification for improved detection of myocardial edema. J Cardiovasc Magn Reson 2009;11:56.
37. Pai A, Li X, Majumdar S. A comparative study at 3 T of sequence dependence of T2 quantitation in the knee. Magn Reson Imaging 2008;26:1215–20.
38. Anderson SW, Sakai O, Soto JA, Jara H. Improved T2 mapping accuracy with dual-echo turbo spin echo: effect of phase encoding profile orders. Magn Reson Med 2013;69:137–43.
39. Poon CS, Henkelman RM. Practical T2 quantitation for clinical applications. J Magn Reson Imaging 1992;2:541–53.
40. Lee MA, Smith S, Palace J, Matthews PM. Defining multiple sclerosis disease activity using MRI T2-weighted difference imaging. Brain 1998; 121:2095–102.
41. Lu H, Nagae-Poetscher LM, Golay X, Lin D, Pomper M, van Zijl PC. Routine clinical brain MRI sequences for use at 3.0 Tesla. J Magn Reson Imaging 2005;22:13–22.

Published OnlineFirst April 21, 2015; DOI: 10.1158/1078-0432.CCR-14-2862

Clinical Cancer Research

Quantification of Nonenhancing Tumor Burden in Gliomas Using Effective T_2 Maps Derived from Dual-Echo Turbo Spin-Echo MRI

Benjamin M. Ellingson, Albert Lai, Huytram N. Nguyen, et al.

Clin Cancer Res 2015;21:4373-4383. Published OnlineFirst April 21, 2015.